**MODELLING OF ACOUSTODIFFUSIVE SURFACE WAVES IN
PIEZOELECTRIC-SEMICONDUCTOR COMPOSITE STRUCTURES**

J. N. Sharma, K. K. Sharma and Ashwani Kumar

msp

MODELLING OF ACOUSTODIFFUSIVE SURFACE WAVES IN PIEZOELECTRIC-SEMICONDUCTOR COMPOSITE STRUCTURES

J. N. SHARMA, K. K. SHARMA AND ASHWANI KUMAR

We investigate the propagation of interfacial surface waves in a composite consisting of homogeneous isotropic semiconductor halfspace coated with a thin layer of homogeneous, transversely isotropic, piezoelectric material. The mathematical model of the problem consists of a coupled system of partial differential equations of motion, diffusion of electrons, and a Gauss equation along with the boundary conditions to be satisfied at the interface and free surface of the composite structure.

The secular equation that governs the wave propagation at the interface has been obtained in compact form after solving the mathematical model analytically. The secular equations in the case of stress-free, isoconcentrated and stress-free, impermeable semiconductor halfspaces have also been deduced as special cases. The complex secular equation has been solved using the functional iteration method along with the irreducible Cardano's method via MATLAB programming for CdSe-Si, CdSe-Ge, PZT-Si and PZT-Ge composite structures.

The computer-simulated results have been presented graphically in terms of phase velocity, attenuation coefficient, and specific loss factor of energy dissipation versus wave number and lifetime of charge carrier field in the considered structures. The work may be useful for the construction and design of surface acoustic wave devices.

1. Introduction

Surface acoustic waves bonded to piezoelectric surfaces have found significant use in various branches of science and technology, especially in the case of interconnected physical fields. These waves were first discovered by Rayleigh [1885], who explained their propagation and characteristics. In [White 1967], the phenomena of surface elastic wave propagation, transduction, and amplification in a piezoelectric semiconductor with special emphasis in relation to electronic devices were discussed. In [Bleustein 1968] the propagation of surface acoustic waves at the free surface of a piezoelectric halfspace was predicted. Gulyaev [1969] explained that a pure transverse wave can propagate along the surface of a homogeneous piezoelectric solid with polarization vector parallel to the surface of the substrate. In [de Lorenzi and Tiersten 1975; Maugin and Daher 1986] nonlinear theories for deformable semiconductors were developed.

Maruszewski [1989] analyzed the effect of interactions between elastic, thermal, and charge carrier fields on Rayleigh waves in addition to electron longitudinal waves in semiconductors. In [Sharma and Thakur 2006] a detailed account of plane harmonic generalised elastothermodiffusive waves in

semiconductor materials was given, suggesting that there are significant modifications in the phase velocities and attenuation coefficients of these waves due to the interactions of mechanical, thermal, and charge carrier fields. In [Sharma and Pathania 2006] the thermoelastic waves in coated homogeneous anisotropic materials were studied to show that anisotropy has significant effect on the phase velocity and attenuation profiles. In [Sharma et al. 2007] it was found that the age of carrier fields also effects wave propagation in semiconductor materials. In [Sharma et al. 2009] it was observed that semiconductor materials exhibit more internal friction with the age of the carrier fields than that of thermal relaxation time. In [Sharma and Pal 2004] the Lamb wave propagation in a transversely isotropic piezothermoelastic plate was investigated. In [Sharma et al. 2010] the propagation of surface waves in a piezoelectric halfspace coated with a semiconductor layer was analyzed.

In [Kagan 1997] the surface wave propagation in a piezoelectric crystal underlying a conducting layer was considered. It was predicted that the electric field excited by the wave in crystal would penetrate into the conducting layer. In [Wang and Varadan 2002] the dispersion characteristics and mode shapes of wave propagation in a piezoelectric layer bonded to the metal substrate were studied. In [Wang 2002] an investigation was conducted into wave propagation in a semiinfinite metallic surface bonded to a layer of piezoelectric material. It was found that the piezoelectric effects dominated the dispersive characteristics at higher wave numbers.

Trolier-Mckinstry and Muralt [2004] explained that thin-film piezoelectric materials offer a number of advantages in microelectromechanical systems and the resulting properties are dominantly dependant on the characteristics of piezoelectric film. In [Du et al. 2007] the Love waves in a functionally graded material layer bonded to a semiinfinite, homogeneous solid were investigated. It was observed that the material properties enable Love waves to propagate along the surface of the layer and may be useful in reducing the dimension of surface acoustic wave (SAW) devices. Jin et al. [2002] studied the Lamb wave propagation in a metallic semiinfinite medium covered with a piezoelectric layer. It was found that the dispersion curves are asymptotic to the transverse velocity of the piezoelectric layer with increasing wave number. In [Melkumyan and Mai 2009] shear surface waves guided by a gap between dissimilar piezoelectric halfspaces were studied. It was concluded that the gap waves were mainly concentrated at the interface of the piezoelectric halfspaces and decayed exponentially away from it. In [Liu et al. 2004] the propagation of surface acoustic waves in a layered halfspace were analyzed, finding that the maximum change in phase velocity occurs for large values of the product of wave number and film thickness.

The design and micromachining of PZT/CdSe thin-layered composites for device applications requires more research in future. Therefore, it is worth investigating the wave propagation parameters in these materials. Keeping in view the wide range applications of composite structures and the above-referred work, an attempt has been made here to study the propagation of surface waves at the interface of a piezoelectric-semiconductor composite structure. The phase velocity, attenuation coefficient, and specific loss factor of energy dissipation for different modes of wave propagation have been computed numerically from the analytically developed model in four types of composite structures: CdSe-Si, PZT-Si, CdSe-Ge, and PZT-Ge. The effect of carrier lifetime has also been taken into account.

The present study shows that PZT-Ge is a good combination for piezoelectric-semiconductor device applications. According to [Muralt and Baborowski 2004] such composites can find applications in ultrasonic transducers and acoustic sensors.

2. Formulation of the problem

Consider a homogeneous isotropic semiconductor halfspace whose surface is coated with a thin layer of homogeneous, transversely isotropic, piezoelectric material of thickness h as shown in Figure 1. The origin of the coordinate system $O - xyz$ is taken at any point on the interface plane and the z-axis points vertically downward into the semiconductor halfspace. Thus, the semiconductor halfspace is represented by $z \geq 0$ and the piezoelectric layer occupies the region $-h \leq z \leq 0$ whose poling direction also aligns along the z-axis. The x-axis is chosen along the direction of wave propagation in such a way that all particles on the line parallel to the y-axis are equally displaced. Therefore, all the field quantities are independent of the y-coordinate and hence we restrict our investigation to the plane strain problem only.

Further, the disturbance is assumed to be confined in the neighborhood of the interface ($z = 0$), and hence vanishes as $z \to \infty$. The basic governing equations of motion, Gauss equation, and electron diffusion for the composite structure under study, in the absence of body forces and electric sources, are given below.

(i) Homogeneous isotropic n-type semiconductor halfspace [Maruszewski 1989; Sharma et al. 2007]:

$$\mu \nabla^2 \vec{u}^s + (\lambda + \mu) \nabla \nabla \cdot \vec{u}^s - \lambda^n \nabla N = \rho^s \ddot{\vec{u}}^s, \tag{1}$$

$$\rho^s D^n \nabla^2 N - \rho^s \left(1 + t^n \frac{\partial}{\partial t}\right) \dot{N} - a_2^n T_0 \lambda^T \nabla \cdot \dot{\vec{u}}^s = -\left(1 + t^n \frac{\partial}{\partial t}\right)\left(\frac{\rho^s}{t_n^+}\right) N. \tag{2}$$

(ii) Homogeneous transversely isotropic piezoelectric (6 mm class) layer [Sharma and Pal 2004]:

$$c_{11} u_{,xx}^P + c_{44} u_{,zz}^P + (c_{13} + c_{44}) w_{,xz}^P + (e_{15} + e_{31}) \phi_{,xz}^P = \rho^P \ddot{u}^P, \tag{3}$$

$$(c_{13} + c_{44}) u_{,xz}^P + c_{44} w_{,xx}^P + c_{33} w_{,zz}^P + e_{15} \phi_{,xx}^P + e_{33} \phi_{,zz}^P = \rho^P \ddot{w}^P, \tag{4}$$

$$(e_{15} + e_{31}) u_{,xz}^P + e_{15} w_{,xx}^P + e_{33} w_{,zz}^P - \varepsilon_{11} \phi_{,xx}^P - \varepsilon_{33} \phi_{,zz}^P = 0, \tag{5}$$

where the notation $\nabla^2 = \partial^2/\partial x^2 + \partial^2/\partial z^2$, $N = n - n_0$, $a_2^n = a^{Qp}/a^Q$, and $\lambda^T = (3\lambda + 2\mu)\alpha_T$ is used. Here λ and μ are Lamè parameters, ρ^s is the density, λ^n are the elastodiffusive constants of electrons, D^n are the diffusion coefficients of electrons, t_n^+ and t^n are the life and relaxation times of the carriers fields, n_0 and n are the equilibrium and nonequilibrium values of electron concentration, and α_T is the coefficient of linear thermal expansion of the semiconductor material. The quantities a^{Qp} and a^Q are flux-like constants and T_0 is the uniform temperature; $\vec{u}^s = (u^s, 0, w^s)$ and $\vec{u}^p = (u^p, 0, w^p)$ are the displacement vectors for semiconductor and piezoelectric materials, respectively. The quantities ϕ^p, ρ^p, c_{ij}, and e_{ij} are the electric potential, density, elastic parameters, and piezoelectric constants, respectively; ε_{11} and
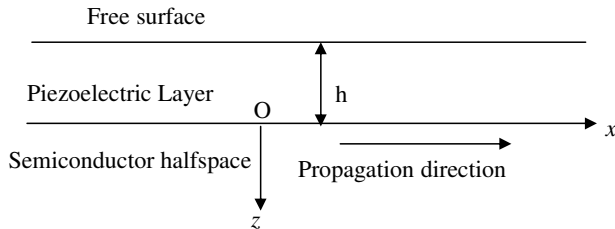

Figure 1. Geometry of the problem.

ε_{33} are the electric permittivity perpendicular to and along the axis of symmetry of the piezoelectric material, respectively.

In the above equations the superposed dots on various quantities denote time differentiation and comma notation is used for spatial derivatives. Throughout this paper the superscripts p and s on the field quantities and material parameters refer to piezoelectric and semiconductor materials, respectively.

The nonvanishing components of stresses, current density, and electric displacement in both the media are

$$\tau_{zz}^s = (\lambda + 2\mu)\frac{\partial w^s}{\partial z} + \lambda\frac{\partial u^s}{\partial x} - \lambda^n N, \quad \tau_{xz}^s = \mu\left(\frac{\partial u^s}{\partial z} + \frac{\partial w^s}{\partial x}\right), \quad J_z^s = -eD^n N_{,z}, \tag{6}$$

for the semiconductor medium and

$$\tau_{zz}^p = c_{13}\frac{\partial u^p}{\partial x} + c_{33}\frac{\partial w^p}{\partial z} + e_{33}\frac{\partial \phi^p}{\partial z},$$

$$\tau_{xz}^p = \frac{c_{44}}{2}\left(\frac{\partial u^p}{\partial z} + \frac{\partial w^p}{\partial x}\right) + e_{15}\frac{\partial \phi^p}{\partial x}, \tag{7}$$

$$D_z^p = e_{31}\frac{\partial u^p}{\partial x} + e_{33}\frac{\partial w^p}{\partial z} - \varepsilon_{33}\frac{\partial \phi^p}{\partial z},$$

in the case of the piezoelectric material. Here τ_{ij}^s and τ_{ij}^p are the stress tensors. The quantities J_z^s and $N_{,z}$ respectively denote the current density and carrier density gradient in the semiconductor material; D_z^p is the electric displacement vector of the piezoelectric material and e is the electronic charge.

2.1. Boundary conditions. The requirement of continuity of stresses, displacements, electric field, and current density at the interface ($z = 0$) of the two media leads to the following interfacial boundary conditions:

$$\tau_{zz}^p = \tau_{zz}^s, \quad \tau_{xz}^p = \tau_{xz}^s, \quad u^p = u^s, \quad w^p = w^s, \quad \phi^p = N, \quad D_z^p = J_z^s. \tag{8}$$

Also the surface ($z = -h$) of the piezoelectric material is assumed to be stress-free and charge-free, which leads to the conditions

$$\tau_{zz}^p = 0, \quad \tau_{xz}^p = 0, \quad D_z^p = 0. \tag{9}$$

In order to simplify the above model, we define the following dimensionless quantities:

$$x' = \frac{\omega^* x}{v_l}, \qquad z' = \frac{\omega^* z}{v_l}, \qquad t' = \omega^* t, \qquad t^{n'} = \omega^* t^n,$$

$$t_n^{+'} = \omega^* t_n^+, \qquad N' = \frac{N}{n_0}, \qquad D_z^{p'} = \frac{\rho^s v_l^2}{\lambda^n n_0 e_{33}} D_z^p, \qquad u^{s'} = \frac{\rho^s \omega^* v_l}{\lambda^n n_0} u^s,$$

$$w^{s'} = \frac{\rho^s \omega^* v_l}{\lambda^n n_0} w^s, \qquad u^{p'} = \frac{\rho^s \omega^* v_l}{\lambda^n n_0} u^p, \qquad w^{p'} = \frac{\rho^s \omega^* v_l}{\lambda^n n_0} w^p, \qquad \tau_{ij}^{p'} = \frac{\tau_{ij}^p}{\lambda^n n_0},$$

$$\tau_{ij}^{s'} = \frac{\tau_{ij}^s}{\lambda^n n_0}, \qquad J_z^{s'} = \frac{J_z^s}{en_0 v_l}, \qquad c_1 = \frac{c_{33}}{c_{11}}, \qquad c_2 = \frac{c_{44}}{c_{11}},$$

$$c_3 = \frac{c_{13}+c_{44}}{c_{11}}, \qquad e_1 = \frac{e_{15}+e_{31}}{e_{33}}, \qquad v_l^2 = \frac{\lambda+2\mu}{\rho^s}, \qquad e_2 = \frac{e_{15}}{e_{33}},$$

$$\bar{\varepsilon} = \frac{\varepsilon_{11}}{\varepsilon_{33}}, \qquad \eta_3 = \frac{\varepsilon_{33}c_{11}}{e_{33}^2}, \qquad \omega' = \frac{\omega}{\omega^*}, \qquad c' = \frac{c}{v_l},$$

$$v_p = \sqrt{\frac{c_{11}}{\rho^p}}, \qquad \bar{\rho} = \frac{\rho^p}{\rho^s}, \qquad \bar{\lambda}_n = \frac{\lambda^n n_0}{\lambda^T T_0}, \qquad \delta_1^2 = \frac{v_l^2}{v_p^2},$$

$$\phi^{p'} = \varepsilon_p \phi^p, \qquad \varepsilon_p = \frac{e_{33}\omega^* \rho^s v_l}{c_{11}\lambda^n n_0}, \qquad \varepsilon_n = \frac{a_2^n \lambda^{T^2} T_0 \bar{\lambda}_n}{\rho^s(\lambda + 2\mu)n_0}, \qquad \omega^* = \frac{v_l^2}{D^n}, \tag{10}$$

$$\delta^2 = \frac{v_t^2}{v_l^2}, \qquad v_t^2 = \frac{\mu}{\rho^s}.$$

Here ω^* is the characteristic frequency and v_l and v_t are, respectively, the longitudinal and shear wave velocities.

On substituting quantities (10) in (1)–(7), we obtain

$$\delta^2 \nabla^2 \vec{u}^s + (1 - \delta^2)\nabla\nabla \cdot \vec{u}^s - \nabla N = \ddot{\vec{u}}^s, \tag{11}$$

$$\nabla^2 N - \left[-\frac{1}{t_n^+} + \left(1 - \frac{t^n}{t_n^+}\right)\frac{\partial}{\partial t} + t^n \frac{\partial^2}{\partial t^2} \right]N - \varepsilon_n \nabla \cdot \dot{\vec{u}}^s = 0, \tag{12}$$

$$u_{,xx}^p + c_2 u_{,zz}^p + c_3 w_{,xz}^p + e_1 \phi_{,xz}^p = \delta_1^2 \ddot{u}^p, \tag{13}$$

$$c_3 u_{,xz}^p + c_2 w_{,xx}^p + c_1 w_{,zz}^p + e_2 \phi_{,xx}^p + \phi_{,zz}^p = \delta_1^2 \ddot{w}^p, \tag{14}$$

$$e_1 u_{,xz}^p + e_2 w_{,xx}^p + w_{,zz}^p - \eta_3 \bar{\varepsilon}\phi_{,xx}^p - \eta_3 \phi_{,zz}^p = 0, \tag{15}$$

$$\tau_{zz}^s = (1 - 2\delta^2)\frac{\partial u^s}{\partial x} + \frac{\partial w^s}{\partial z} - N, \quad \tau_{xz}^s = \delta^2 \left(\frac{\partial u^s}{\partial z} + \frac{\partial w^s}{\partial x}\right), \quad J_z^s = -N_{,z} \tag{16}$$

$$\tau_{zz}^p = \frac{\bar{\rho}}{\delta_1^2}\left\{(c_3 - c_2)\frac{\partial u^p}{\partial x} + c_1 \frac{\partial w^p}{\partial z} + \phi_{,z}^p\right\}, \quad \tau_{xz}^p = \frac{\bar{\rho}}{\delta_1^2}\left\{\frac{c_2}{2}\left(\frac{\partial u^p}{\partial z} + \frac{\partial w^p}{\partial x}\right) + e_2\phi_{,x}^p\right\},$$

$$D_z^p = (e_1 - e_2)\frac{\partial u^p}{\partial x} + \frac{\partial w^p}{\partial z} - \eta_3 \phi_{,z}^p. \tag{17}$$

The scalar and vector point potential functions ϕ^s and ψ^s in the semiconductor medium through the relations are introduced as

$$u^s = \frac{\partial \phi^s}{\partial x} + \frac{\partial \psi^s}{\partial z}, \quad w^s = \frac{\partial \phi^s}{\partial z} - \frac{\partial \psi^s}{\partial x}, \tag{18}$$

to facilitate the solutions in semiconductor material.

Using relations (18) in (11) and (12), we obtain

$$\nabla^2 \phi^s - N - \ddot{\phi}^s = 0, \tag{19}$$

$$\nabla^2 \psi^s = \frac{\ddot{\psi}^s}{\delta^2}, \tag{20}$$

$$\nabla^2 N - \left[-\frac{1}{t_n^+} + \left(1 + \frac{t^n}{t_n^+}\right)\frac{\partial}{\partial t} + t^n \frac{\partial^2}{\partial t^2} \right]N - \varepsilon_n \nabla^2 \dot{\phi}^s = 0. \tag{21}$$

Equation (20) corresponds to purely transverse waves in the semiconductor which get decoupled from rest of the motion and are not affected by the charge carrier fields.

3. Formal solution of the problem

We assume the harmonic wave solution of the form

$$(\psi^s, \phi^s, N, u^p, w^p, \phi^p) = (\bar{\psi}^s, \bar{\phi}^s, \bar{N}, \bar{u}^p, \bar{w}^p, \bar{\phi}^p) \exp\{ik(x - ct)\}, \tag{22}$$

where $c = \omega/k$ is the phase velocity and k and ω are the wave number and angular frequency, respectively.

Upon imposing solution (22) in (13)–(15) and (19)–(21), straightforward algebraic simplifications lead to the following formal solution satisfying the radiation conditions in both the media:

(i) Semiconductor (n-type) halfspace ($z \geq 0$):

$$(\phi^s, N) = \sum_{i=1}^{2} (1, S_i) A_i^s e^{-n_i z} \exp\{ik(x - ct)\}, \quad \psi^s = A_3^s \exp\{-\beta z + ik(x - ct)\}. \tag{23}$$

(ii) Piezoelectric (6 mm class) layer $0 \leq z \leq -h$:

$$u^p = \sum_{i=1}^{3} (A_i^p e^{m_i z} + B_i^p e^{-m_i z}) \exp\{ik(x - ct)\},$$

$$(w^p, \phi^p) = \sum_{i=1}^{3} (M_i, P_i)(A_i^p e^{m_i z} - B_i^p e^{-m_i z}) \exp\{ik(x - ct)\}, \tag{24}$$

where

$$\alpha^2 = k^2(1 - c^2), \qquad S_i = n_i^2 - \alpha^2, \qquad n_i^2 = k^2(1 - c^2 a_i^2), \quad i = 1, 2,$$

$$\beta^2 = k^2\left(1 - \frac{c^2}{\delta^2}\right), \qquad \xi = (1 - \delta_1^2 c^2), \tag{25}$$

$$A = (c_1\bar{\varepsilon} + c_2 - \delta_1^2 c^2)\eta_3 + 2e_2, \qquad\qquad B = (c_2 - \delta_1^2 c^2)\eta_3\bar{\varepsilon} + e_2^2,$$

$$a_1^2 + a_2^2 = 1 + t^n + i\omega^{-1}\left(1 + \varepsilon_n - \frac{t^n}{t_n^+}\right) + \frac{1}{\omega^2 t_n^+}, \qquad a_1^2 a_2^2 = t^n + i\omega^{-1}\left(1 - \frac{t^n}{t_n^+}\right) + \frac{1}{\omega^2 t_n^+}, \tag{26}$$

$$m_1^2 m_2^2 + m_2^2 m_3^2 + m_3^2 m_1^2 = k^4 \frac{c_2 B + \xi A - c_3(c_2\eta_3\bar{\varepsilon} + 2e_1 e_2) + e_1^2(c_2 - \delta_1^2 c^2)}{c_2(1 + \eta_3 c_1)},$$

$$m_1^2 + m_2^2 + m_3^2 = k^2 \frac{c_2 A + \xi(1 + \eta_3 c_1) - c_3(c_3\eta_3 + 2e_1) + c_1 e_1^2}{c_2(1 + \eta_3 c_1)}, \qquad m_1^2 m_2^2 m_3^2 = k^6 \frac{\xi B}{c_2(1 + \eta_3 c_1)}, \tag{27}$$

$$M_i = \frac{-ikm_i\{c_3\eta_3(m_i^2 - k^2\bar{\varepsilon}) + e_1(m_i^2 - k^2 e_2)\}}{(c_1 m_i^2 - k^2 c_2 + \delta_1^2 k^2 c^2)(m_i^2 - k^2\bar{\varepsilon})\eta_3 + (m_i^2 - k^2 e_2)^2}, \quad i = 1, 2, 3,$$

$$P_i = \frac{ike_1 m_i}{\eta_3(m_i^2 - k^2\bar{\varepsilon})} + \frac{(m_i^2 - k^2 e_2)}{\eta_3(m_i^2 - k^2\bar{\varepsilon})} M_i, \quad i = 1, 2, 3. \tag{28}$$

Substituting the solutions (23) in (16) and (18), we obtain the normal stress, shear stress, current density, and displacements for the semiconductor material as

$$\tau_{zz}^s = \left(p \sum_{i=1}^{2} A_i^s e^{-n_i z} + q A_3^s e^{-\beta z} \right) \exp\{ik(x - ct)\}, \tag{29}$$

$$\tau_{xz}^s = \left(-\sum_{i=1}^{2} f_i A_i^s e^{-n_i z} + p A_3^s e^{-\beta z} \right) \exp\{ik(x - ct)\}, \tag{30}$$

$$J_z^s = \sum_{i=1}^{2} S_i n_i A_i^s \exp\{-n_i z + ik(x - ct)\}, \tag{31}$$

$$u^s = \left(ik \sum_{i=1}^{2} A_i^s e^{-n_i z} - \beta A_3^s e^{-\beta z} \right) \exp\{ik(x - ct)\}, \tag{32}$$

$$w^s = -\left(\sum_{i=1}^{2} n_i A_i^s e^{-n_i z} + ik A_3^s e^{-\beta z} \right) \exp\{ik(x - ct)\}, \tag{33}$$

where

$$p = \delta^2(k^2 + \beta^2), \quad q = 2ik\delta^2\beta, \quad f_i = 2ik\delta^2 n_i \ (i = 1, 2), \quad A_i^s \ (i = 1, 2, 3)$$

are the unknowns to be determined. Similarly, we obtain expressions for normal stress, shear stress, and electric displacement for the piezoelectric layer by using (24) in (17) as

$$(\tau_{zz}^p, D_z^p) = \sum_{i=1}^{3} \left\{ (y_i, b_i)(A_i^p e^{m_i z} + B_i^p e^{-m_i z}) \exp\{ik(x - ct)\} \right\},$$

$$\tau_{xz}^p = \sum_{i=1}^{3} d_i (A_i^p e^{m_i z} - B_i^p e^{-m_i z}) \exp\{ik(x - ct)\}, \tag{34}$$

where

$$y_i = \frac{\bar{\rho}}{\delta_1^2} \{ik(c_3 - c_2) + c_1 m_i M_i + m_i P_i\}, \quad d_i = \frac{\bar{\rho}}{\delta_1^2} \left\{ \frac{c_2}{2}(m_i + ikM_i) + ike_2 P_i \right\},$$

$$b_i = ik(e_1 - e_2) + m_i(M_i - \eta_3 P_i), \tag{35}$$

and A_i^p and B_i^p $(i = 1, 2, 3)$ are the unknowns to be determined.

4. Secular equation

Considering the formal solution for various field quantities obtained in the previous section and employing the boundary conditions (8) and (9), we obtain a system of nine coupled homogeneous algebraic equations in nine unknowns A_i^s, A_i^p, and B_i^p $(i = 1, 2, 3)$. This system has a nontrivial solution if the determinant of the coefficients of A_i^s, A_i^p, and B_i^p $(i = 1, 2, 3)$ vanishes. After lengthy algebraic reductions and simplifications, the secular equation for the propagation of guided waves in the considered

composite structure is obtained as

$$\tanh(m_1 h) = \frac{g_{12}(g_{21}g_{33} - g_{31}g_{23}) - g_{13}(g_{21}g_{32} - g_{31}g_{22})}{g_{11}(g_{22}g_{33} - g_{32}g_{23})}, \tag{36}$$

where

$$g_{11} = b_{21}b_{14} - \frac{b_{11}b_{24}}{\sinh(m_1 h)}, \qquad g_{1i} = \frac{b_{2i}b_{14} - b_{1i}b_{24}}{\cosh(m_1 h)}, \quad i = 2, 3,$$

$$g_{2i} = b_{3i}b_{14} - b_{1i}b_{34}, \qquad i = 1, 2, 3, \qquad g_{3i} = b_{4i}b_{14} - b_{1i}b_{44}, \quad i = 1, 2, 3. \tag{37}$$

Here b_{ij} $(i, j = 1, 2, 3, 4)$ are given by

$$b_{1i} = a_{3i}(a_{25}a_{16} - a_{15}a_{26}) - a_{2i}(a_{35}a_{16} - a_{15}a_{36}), \qquad\qquad i = 1, 2,$$

$$b_{1j} = (a_{3j}a_{16} - a_{1j}a_{36})(a_{25}a_{16} - a_{15}a_{26}) - (a_{2j}a_{16} - a_{1j}a_{26})(a_{35}a_{16} - a_{15}a_{36}), \qquad j = 3, 4,$$

$$b_{21} = a_{41}(a_{25}a_{16} - a_{15}a_{26}) - \frac{a_{21}(a_{45}a_{16} - a_{15}a_{46})}{\sinh(m_1 h)},$$

$$b_{22} = a_{42}(a_{25}a_{16} - a_{15}a_{26}) - a_{22}(a_{45}a_{16} - a_{15}a_{46}),$$

$$b_{2j} = (a_{4j}a_{16} - a_{1j}a_{46})(a_{25}a_{16} - a_{15}a_{26}) - (a_{2j}a_{16} - a_{1j}a_{26})(a_{45}a_{16} - a_{15}a_{46}), \qquad j = 3, 4, \tag{38}$$

$$b_{3i} = a_{5i}(a_{25}a_{16} - a_{15}a_{26}) - a_{2i}(a_{55}a_{16} - a_{15}a_{56}), \qquad\qquad i = 1, 2,$$

$$b_{3j} = (a_{5j}a_{16} - a_{1j}a_{56})(a_{25}a_{16} - a_{15}a_{26}) - (a_{2j}a_{16} - a_{1j}a_{26})(a_{55}a_{16} - a_{15}a_{56}), \qquad j = 3, 4,$$

$$b_{4i} = a_{6i}(a_{25}a_{16} - a_{15}a_{26}) - a_{2i}(a_{65}a_{16} - a_{15}a_{66}), \qquad\qquad i = 1, 2,$$

$$b_{4j} = (a_{6j}a_{16} - a_{1j}a_{66})(a_{25}a_{16} - a_{15}a_{26}) - (a_{2j}a_{16} - a_{1j}a_{26})(a_{65}a_{16} - a_{15}a_{66}), \qquad j = 3, 4.$$

The quantities a_{ij} $(i, j = 1, \ldots, 6)$ are defined in the Appendix.

5. Solution of secular equation

In general, the wave number and hence the phase velocities of the waves are complex quantities, therefore the waves will be attenuated in space. In order to solve the secular equation (36), we take

$$c^{-1} = V^{-1} + i\omega^{-1}Q, \tag{39}$$

where $k = R + iQ$, $R = \omega/V$, and R and Q are real numbers. Here, it may be noted that V and Q respectively represent the phase velocity and attenuation coefficient of the waves. Using representation (39) in various relevant relations, the complex roots m_i^2 $(i = 1, 2, 3)$ can be computed from (27) with the help of Cardano's method. The roots m_i^2 are further used to solve the secular equation (36) to obtain the phase velocity and attenuation coefficient of the surface waves by using the functional iteration numerical technique outlined below.

In general the secular equation (36) is of the form $c = \phi(c)$ which on using representation (39) leads to a system of two real equations $f(V, Q) = 0$ and $g(V, Q) = 0$. In order to apply the functional iteration method we write $V = f^*(V, Q)$ and $Q = g^*(V, Q)$, where the functions f^* and g^* are selected in such a way that they satisfy the conditions

$$\left|\frac{\partial f^*}{\partial V}\right| + \left|\frac{\partial f^*}{\partial Q}\right| < 1, \qquad \left|\frac{\partial g^*}{\partial V}\right| + \left|\frac{\partial g^*}{\partial Q}\right| < 1, \tag{40}$$

for all V, Q in the neighborhood of the root. If (V_0, Q_0) is an initial approximation of the root, then we can construct the successive approximations according to the formulae

$$
\begin{aligned}
V_1 &= f^*(V_0, Q_0), & Q_1 &= g^*(V_1, Q_0), \\
V_2 &= f^*(V_1, Q_1), & Q_2 &= g^*(V_2, Q_1), \\
&\vdots & &\vdots \\
V_{n+1} &= f^*(V_n, Q_n), & Q_{n+1} &= g^*(V_{n+1}, Q_n).
\end{aligned}
\tag{41}
$$

The sequence (V_n, Q_n) of approximations of the root will converge to the actual root provided (V_0, Q_0) lies in the neighborhood of the actual root. For an initial value of $c = c_0 = (V_0, Q_0)$, the roots m_i ($i = 1, 2, 3$) are computed from (27) by using Cardano's method for each value of the nondimensional wave number (R) for the assigned frequency. The values of m_i so obtained are then used in the secular equation (36) to find the current values of V and Q each time, which are further used to generate the sequence (41). The process is terminated as and when the condition $|V_{n+1} - V_n| < \varepsilon$, ε being an arbitrarily small number to be selected at random in order to achieve the desired accuracy level, is satisfied. The procedure is continuously repeated for different values of nondimensional wave number to obtain the corresponding values of the phase velocity and attenuation coefficient. Thus, the real phase velocity and attenuation coefficient during the propagation of Rayleigh-type waves in the composite structure under study can be computed from the dispersion relation (36).

5.1. *Specific loss*. The specific loss is the direct method of defining the internal friction for a material. According to [Kolsky 1963], in the case of a sinusoidal plane wave of small amplitude, the specific loss $\Delta W / W$ equals 4π times the ratio of the absolute value of the imaginary part of k to the real part of k. Here

$$
\frac{\Delta W}{W} = 4\pi \left| \frac{\operatorname{Im}(k)}{\operatorname{Re}(k)} \right| = 4\pi \left| \frac{Q}{R} \right| = 4\pi \left| \frac{VQ}{\omega} \right|.
\tag{42}
$$

6. Special cases of wave solution

In the case where the piezoelectric layer is absent ($h = 0$), the composite structure reduces to a semiconductor halfspace subjected to stress-free, isoconcentrated or stress-free, impermeable boundary conditions. The secular equation (36) in this case reduces to the following two equations:

$$
(k^2 + \beta^2)^2 (n_1 + n_2) = 4k^2 \beta (n_1 n_2 + \alpha^2),
\tag{43}
$$

$$
(k^2 + \beta^2)^2 (n_1^2 + n_1 n_2 + n_2^2 - \alpha^2) = 4k^2 \beta n_1 n_2 (n_1 + n_2).
\tag{44}
$$

Equation (43) corresponds to the secular equation which governs the surface wave motion in the case of stress-free, isoconcentrated boundary conditions prevailing at the surface of the semiconductor halfspace and (44) refers to the secular equation for the stress-free, impermeable surface of the semiconductor halfspace.

Equations (43) and (44) have similar forms as that of the thermoelastic Rayleigh frequency equation [Maruszewski 1989; Sharma et al. 2007] and hence electron concentration produces the same type of surface effects as the heat flux conduction/heat transfer phenomenon. In the case where electron and

elastic fields are uncoupled ($\varepsilon_n = 0$), from (26) we have

$$a_1^2 = 1, \quad a_2^2 = t^n + i\omega^{-1}\left(1 - \frac{t^n}{t_n^+}\right) + \frac{1}{t_n^+ \omega^2},$$

so that $n_1^2 = \alpha^2$. Consequently (43) and (44) collapse to

$$(k^2 + \beta^2)^2 = 4k^2\alpha\beta. \tag{45}$$

This is the famous Rayleigh frequency equation [Graff 1975] in a stress-free elastic halfspace.

7. Numerical results and discussion

The analytical solutions for various field quantities obtained lead to the transcendental secular equation (36) which contains complete information about the effect of different interacting fields and lifespan of the charge carriers on the phase velocity, attenuation coefficient, and specific loss factor of energy dissipation. In order to illustrate the theoretical results obtained above, we now present some numerical results for four composite structures, namely, CdSe-Si, CdSe-Ge, PZT-Si, and PZT-Ge. The material parameters and constants for the semiconductor halfspace and piezoelectric layer used in the numerical computations are given in Tables 1 and 2, respectively.

The numerical computations were performed by employing the procedure outlined in Section 5 with the help of MATLAB programming. The computations were performed for the first three modes of wave propagation in the considered composite structures. In the following discussion, Rh denotes the nondimensional wave number for surface waves travelling at the interface of the semiconductor halfspace and piezoelectric layer while R represents the wave number for Rayleigh surface waves at the free surface of the semiconductor halfspace.

Figures 2 and 3 present the variations of phase velocity of surface waves at the interface of the composites CdSe-Ge and PZT-Ge, respectively, versus wave number Rh for the first three modes of wave propagation. The waves are noticed to be dispersive in nature in both cases. There is a sharp decrease in the phase velocity at long wavelengths. It is clear that the maximum fall in the phase velocity occurs for $0 \leq Rh \leq 2$. At small wavelengths phase velocity almost attains a constant value for $Rh \geq 2$. Initially the higher modes of wave propagation have large phase velocity as compared to that of lower-order modes. Moreover, the velocity profiles are observed to be similar for the considered composite structures with

Sample number	Quantity	Unit	Si	Ge
1	ρ^s	$Kg\,m^{-3}$	2.3×10^3	5.3×10^3
2	λ	$N\,m^{-2}$	0.64×10^{11}	0.48×10^{11}
3	μ	$N\,m^{-2}$	0.65×10^{11}	0.53×10^{11}
4	D^n	$m^2 s^{-1}$	0.35×10^{-2}	1×10^{-2}
5	n_0	m^{-3}	10^{20}	10^{20}
6	α_T	K^{-1}	2.6×10^{-6}	5.8×10^{-6}

Table 1. Physical data for n-type Si and Ge semiconductors [Maruszewski 1989; Sharma and Thakur 2006].

Sample number	Quantity	Unit	CdSe	PZT-4
1	ρ^p	$\mathrm{kg\,m^{-3}}$	5.504×10^3	7.5×10^3
2	c_{11}	$\mathrm{Nm^{-2}}$	7.41×10^{10}	13.2×10^{10}
3	c_{13}	$\mathrm{Nm^{-2}}$	3.93×10^{10}	7.3×10^{10}
4	c_{33}	$\mathrm{Nm^{-2}}$	8.36×10^{10}	11.5×10^{10}
5	c_{44}	$\mathrm{Nm^{-2}}$	1.32×10^{10}	2.6×10^{10}
6	e_{31}	$\mathrm{Cm^{-2}}$	-0.160	-4.1
7	e_{33}	$\mathrm{Cm^{-2}}$	0.347	14.1
8	e_{15}	$\mathrm{Cm^{-2}}$	-0.138	10.5
9	ε_{11}	$\mathrm{C^2N^{-1}m^{-2}}$	8.26×10^{-11}	7.1×10^{-9}
10	ε_{33}	$\mathrm{C^2N^{-1}m^{-2}}$	9.03×10^{-11}	5.8×10^{-9}
11	ε_0	F/m	8.854×10^{-12}	8.854×10^{-12}

Table 2. Physical data for 6 mm class CdSe [Sharma and Pal 2004] and PZT-4 [Jin et al. 2002] piezoelectric materials.

the exception that phase velocity possesses large magnitude in the case of the PZT-Ge composite as compared to that the CdSe-Ge one. It is worth noting that all the modes of wave propagation start with higher phase velocity at long wavelengths, showing the cutoff frequencies for their existence. The penetration power of the long wavelength surface waves is higher than that of short wavelengths. Thus at long wavelengths the medium gets disturbed to its maximum and the coupling between various interacting fields become operative, thereby increasing the phase velocity and hence the speed of the surface waves. This is in contrast to short-wavelength waves which just follow the surface without much disturbance to the core material. This agrees with the conclusion drawn in [Lowrie 2007].
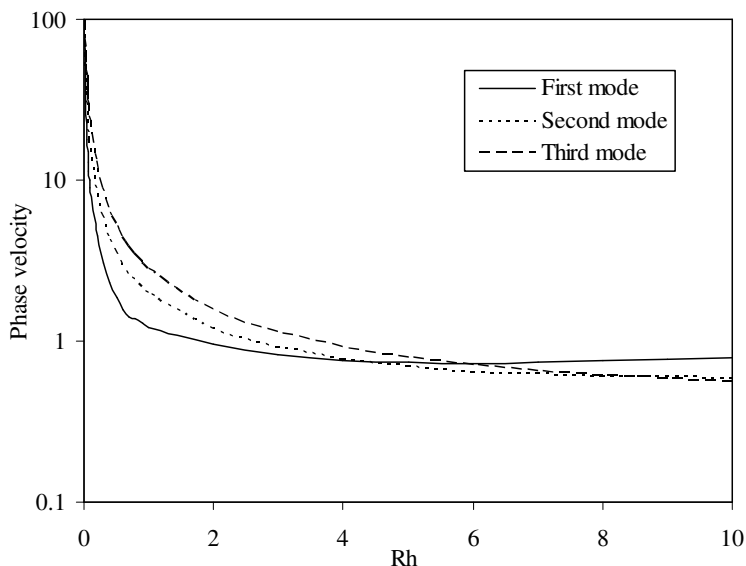
Figure 2. Phase velocity versus *Rh* for CdSe-Ge composite.
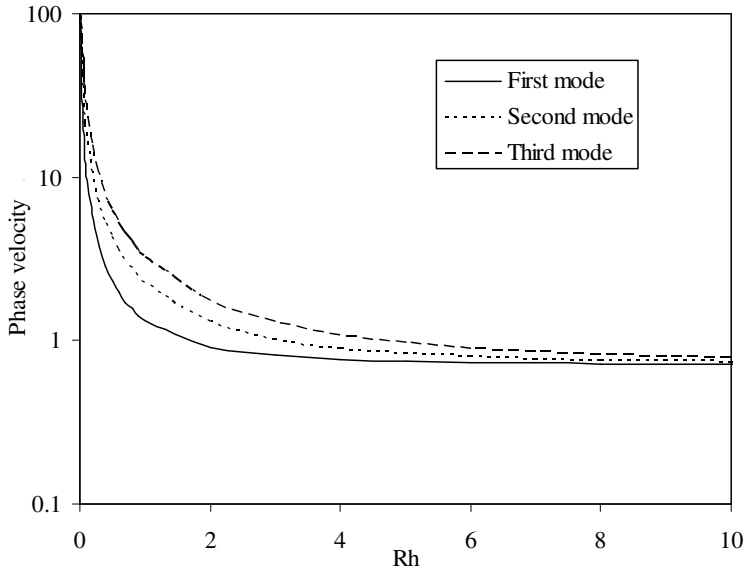
Figure 3. Phase velocity versus Rh for PZT-Ge composite.

Figure 4 shows the variation of the attenuation coefficient with wave number Rh for the CdSe-Ge composite. Here the attenuation coefficient increases with Rh for all the modes. The lower-order modes of wave propagation possess larger attenuation than the higher modes.

Figure 5 presents the variations of the attenuation coefficient with wave number Rh in the PZT-Ge composite. In this case the attenuation coefficient first increases with Rh to attain maximum value and decreases afterwards with Rh. The maxima for attenuation coefficients shift towards larger values of Rh with increasing mode of wave propagation. Moreover, the PZT-Ge composite possesses a smaller
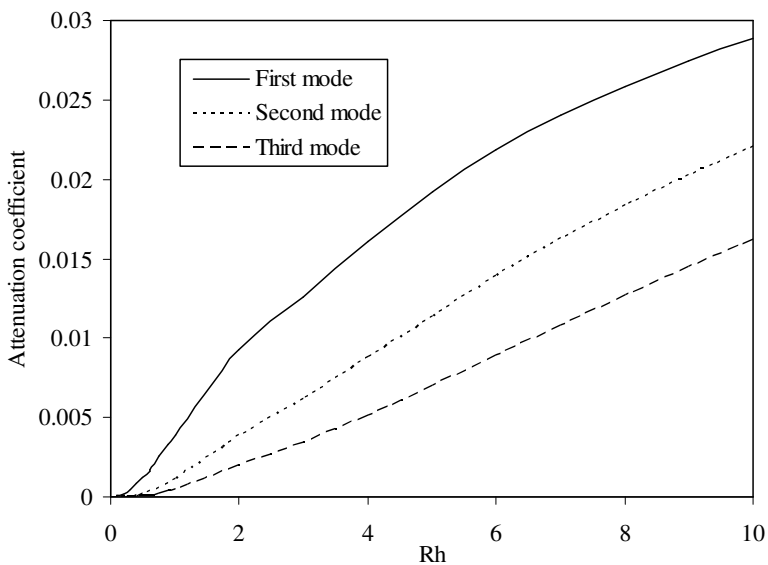
Figure 4. Attenuation coefficient versus Rh for CdSe-Ge composite.
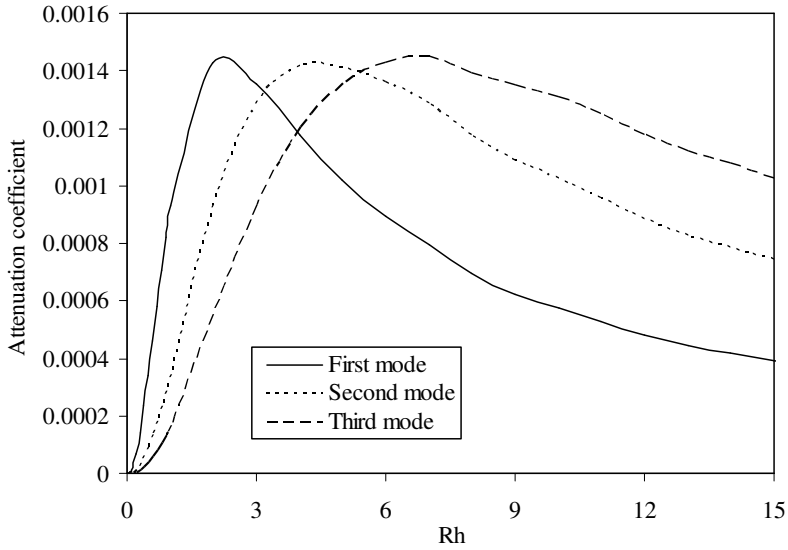
Figure 5. Attenuation coefficient versus *Rh* for PZT-Ge composite.

attenuation coefficient than that of the CdSe-Si composite structure.

Figures 6 and 7 represent the variations of the specific loss factor of energy dissipation with wave number *Rh* in the composites CdSe-Ge and PZT-Ge, respectively. The specific loss factor of waves in these composites follows similar trends as those of their attenuation coefficients. The variations of phase velocity with age of the charge carrier field for all the considered composites are shown in Figure 8. The phase velocity profiles possess almost uniform behaviour with the lifetime except in the CdSe-Ge composite where it has a slightly large value at 0.1 ps in comparison to the neighboring points, which may
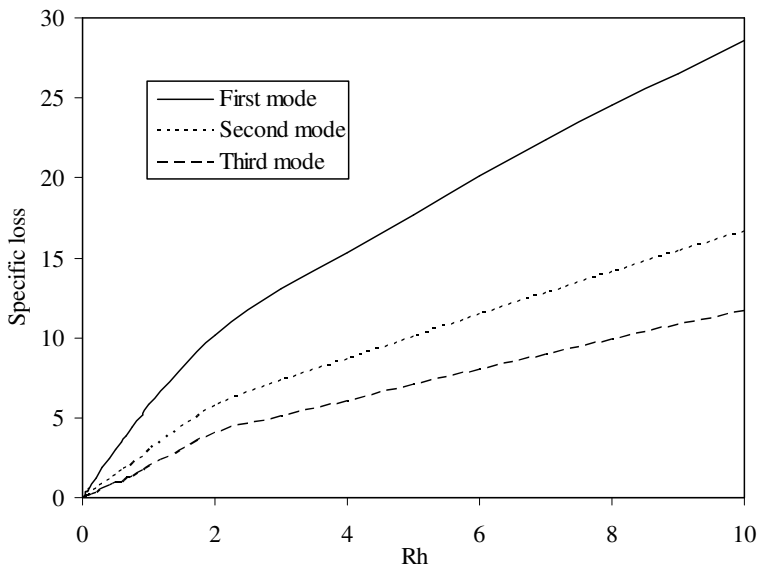
Figure 6. Specific loss versus *Rh* for CdSe-Ge composite.
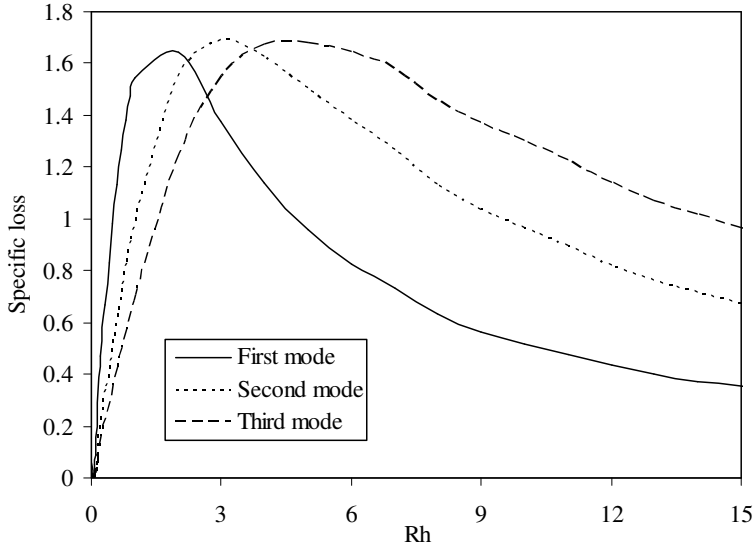
Figure 7. Specific loss versus *Rh* for PZT-Ge composite.

be attributed to numerical instability at that point. It is also evident from the phase velocity profiles that the magnitude of phase velocity is highest for PZT-Ge and lowest in the case of the CdSe-Si composite. Figure 9 shows the variations of the attenuation coefficient with the lifetime of the carrier field in the considered composites. It is evident that for CdSe-Si and CdSe-Ge the magnitude of attenuation has a uniform value up to $t_n^+ = 0.1$ ps and decreases afterwards. However, in the PZT-Ge and PZT-Si composites, the variations of the attenuation coefficient remain almost constant with lifetime. This comparative study reveals that the PZT-Ge composite has the lowest attenuation while the CdSe-Si exhibits the highest
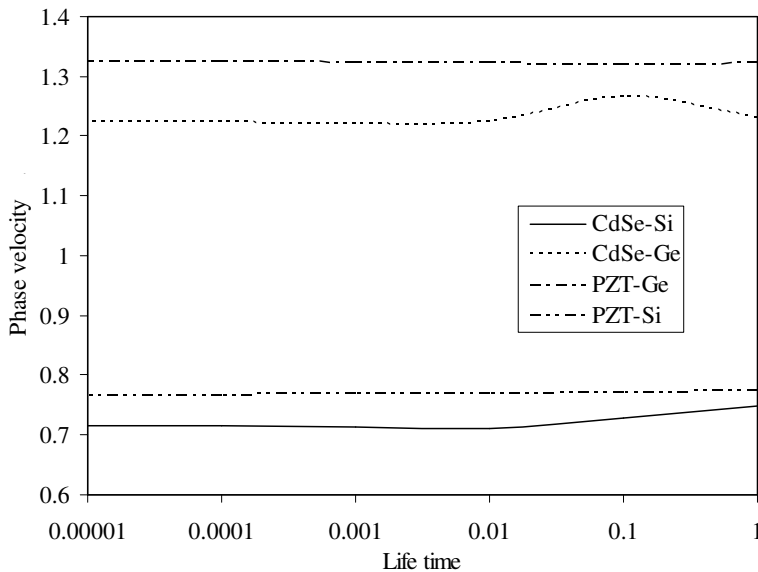
Figure 8. Phase velocity versus lifetime (in ps) of carrier field.
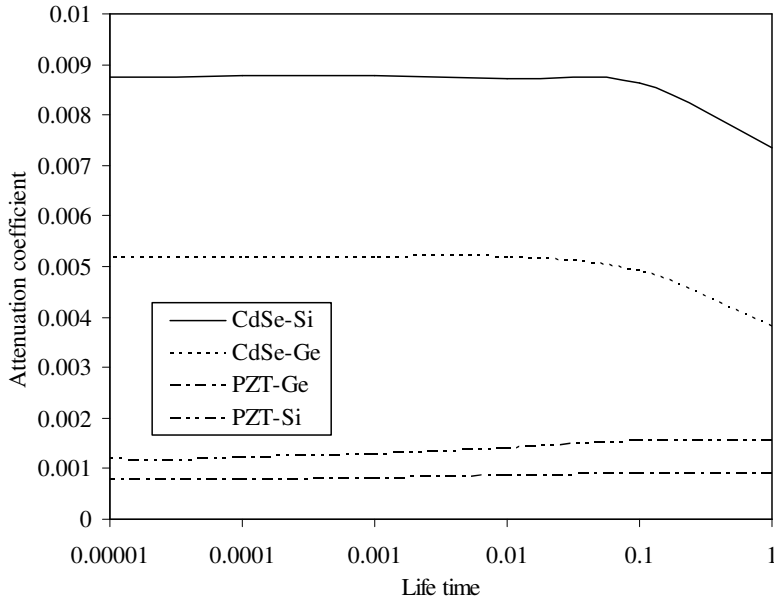
Figure 9. Attenuation coefficient versus lifetime (in ps) of carrier field.

attenuation among all the considered structures. The PZT-Ge composite is a combination of higher density materials in comparison to CdSe-Si, which has low density, and therefore the phase velocity is large in value in the former composite because acoustic waves travel faster in the denser medium than in the rarer one.

Figures 10–14 show the variations of various wave characteristics in the silicon semiconductor half-space. Figure 10 represents the variations of phase velocity with wave number R in the semiconductor
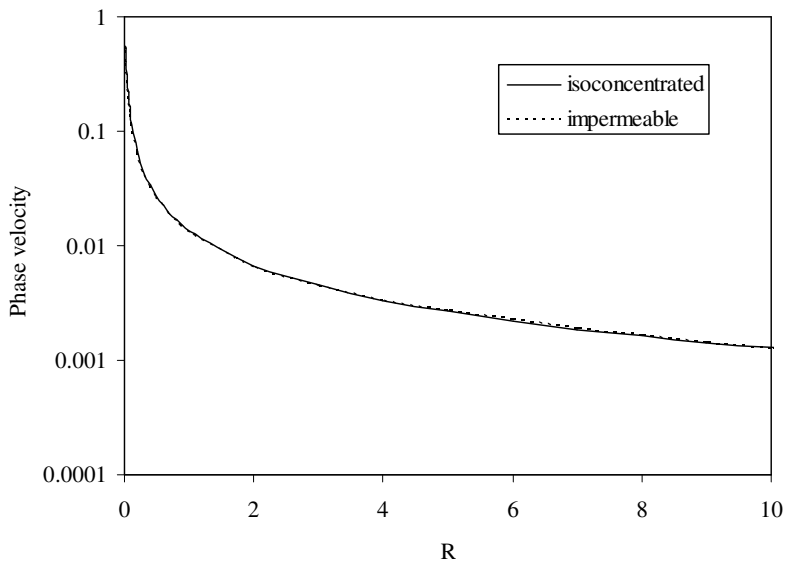
Figure 10. Phase velocity versus R in semiconductor halfspace.
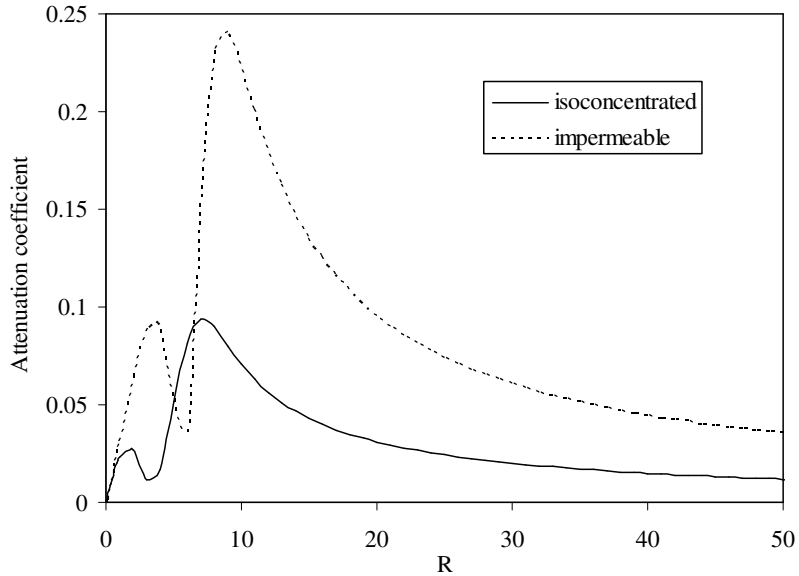
Figure 11. Attenuation coefficient versus R in semiconductor halfspace.

halfspace under stress-free and isoconcentrated as well as stress-free and impermeable boundary conditions. The waves are again attenuated and dispersive in character for the same reason as explained for Figures 2 and 3. However, there is a sharp decay in the phase velocity of these waves in the range $0 \leq R \leq 2$ which attains an almost constant value for $R \geq 2$. It may be noticed that the phase velocities have almost equal magnitudes in the case of both the boundary conditions prevailing at the surface of the semiconductor halfspace. Figure 11 shows the variations of the attenuation coefficient with wave number R for stress-free and isoconcentrated as well as stress-free and impermeable boundary conditions
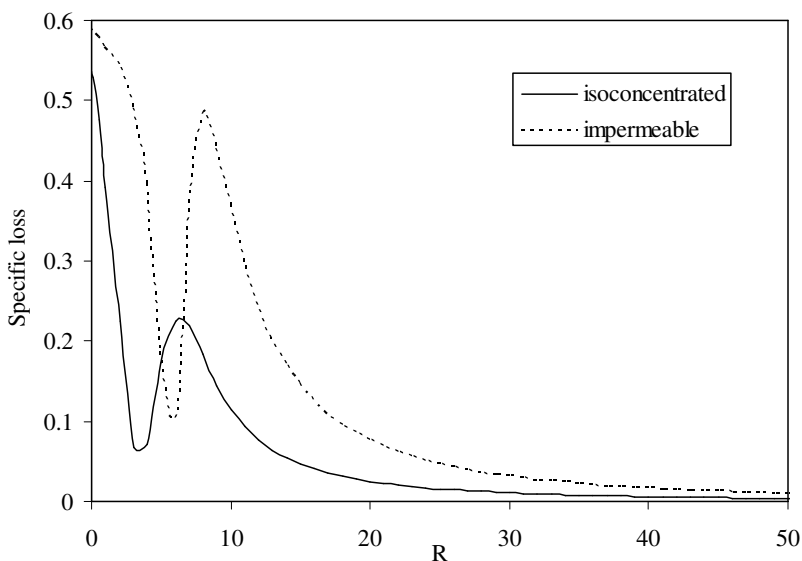
Figure 12. Specific loss versus R in semiconductor halfspace.
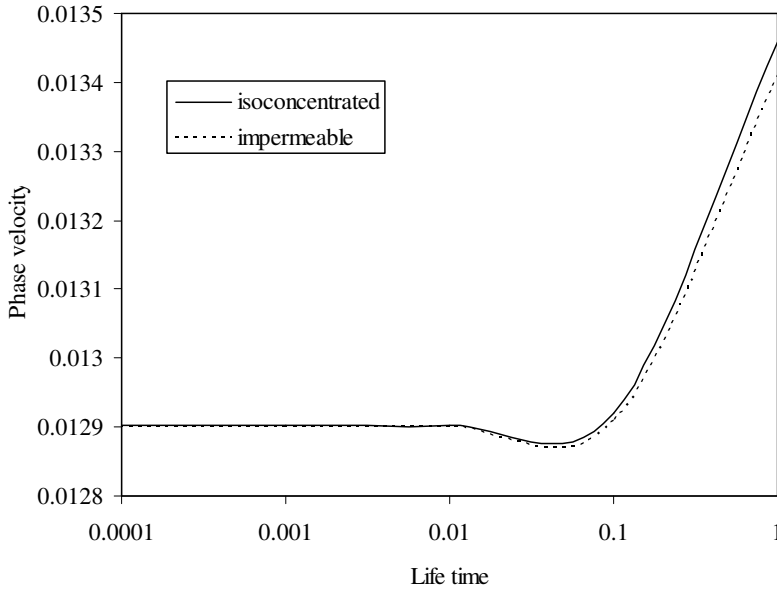
Figure 13. Phase velocity versus lifetime (in ps) of carrier field in semiconductor halfspace.

at the surface of the halfspace. The attenuation coefficient increases in the range $0 \leq R \leq 2$, decreases for $2 \leq R \leq 3$ and again increases for $3 \leq R \leq 7$ before it decreases with R for stress-free and isoconcentrated boundary conditions. Similar trends of variations are also noticed in the case of stress-free and impermeable conditions with the exception that in this case the attenuation has a high magnitude. Figure 12 presents the variations of the specific loss factor of energy dissipation with wave number R. The specific loss factor decreases for $0 \leq R \leq 3$ and increases for $3 \leq R \leq 6$, before it starts decreasing with R in the case of stress-free and isoconcentrated boundary conditions at the surface of the halfspace. In the case of stress-free and impermeable boundary conditions it also follows a similar trend. The specific loss factor has a large magnitude in the case of impermeable conditions as compared to that for the isoconcentrated one. The attenuation and specific loss profiles show some oscillatory behaviour at long wavelengths, which is attributed to the fact that the acoustic waves penetrate significantly deep into the medium under such situations forcing the various coupling parameters of the interacting fields to become operative. Whereas at short wavelengths, both these quantities show smooth behaviour as the waves mainly travel along the surface, causing the least disturbance to the medium. Figure 13 shows the variations of phase velocity with lifetime of the charge carriers in the semiconductor halfspace. Phase velocity remains almost constant up to $t_n^+ = 0.01$ ps and then increases rapidly in the case of both boundary conditions. The generation and recombination of the electrons become more frequent with decreasing lifetime. Moreover, the wave field interaction with the newly generated electron imparts some energy to it, which results in decreasing the phase velocity of the wave. The magnitude of the phase velocity is slightly higher for the stress-free and isoconcentrated boundary conditions as compared to other conditions. The variations of the attenuation coefficient with lifetime for the semiconductor halfspace are shown in Figure 14. The attenuation coefficient decreases with decreasing lifetime for both boundary conditions. The attenuation coefficient has a large magnitude in the case of stress-free and impermeable conditions as compared to that for stress-free and isoconcentrated conditions for $t_n^+ \geq 0.1$ ps.
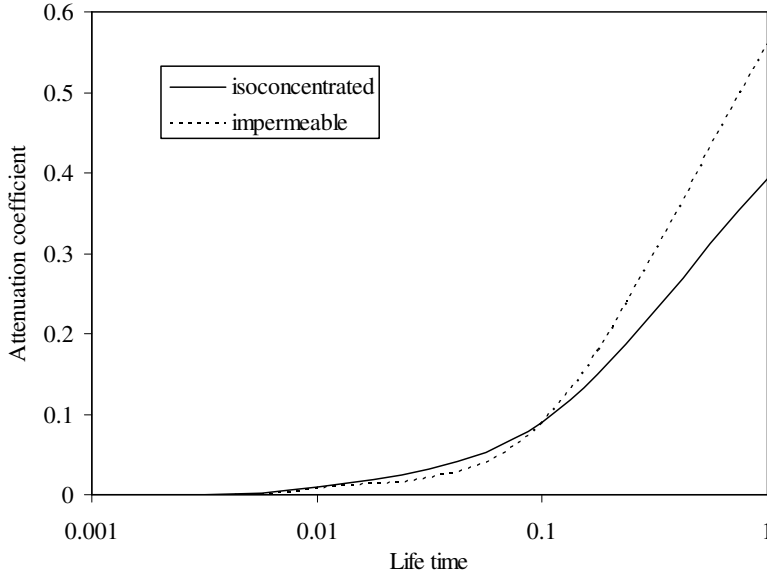
Figure 14. Attenuation coefficient versus lifetime (in ps) in semiconductor halfspace.

Figures 15 and 16 show the plots of computer-simulated results in respect of phase velocities and attenuation coefficients of first mode of wave propagation at $t_n^+ = 1$ ps in all the considered structures. Close inspection of the phase velocity and attenuation coefficient profiles in Figures 15 and 16 reveals that for the same choice of patch/core material in the composite structure, these quantities follow similar trends in their variations. It is clear that the phase velocity decreases from its initial high value at long wavelengths to become steady at short wavelengths in all the composites. The phase velocity has a large
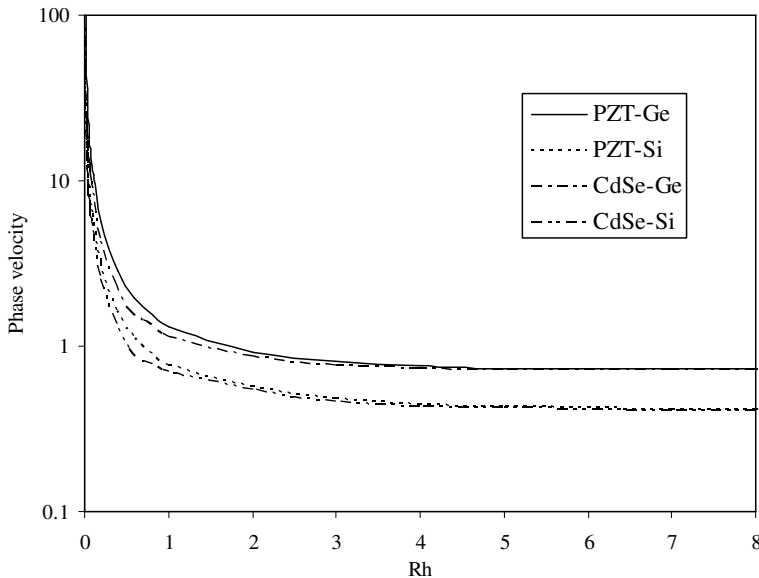
Figure 15. Phase velocity versus *Rh* for PZT-Ge, PZT-Si, CdSe-Ge, and CdSe-Si composites.
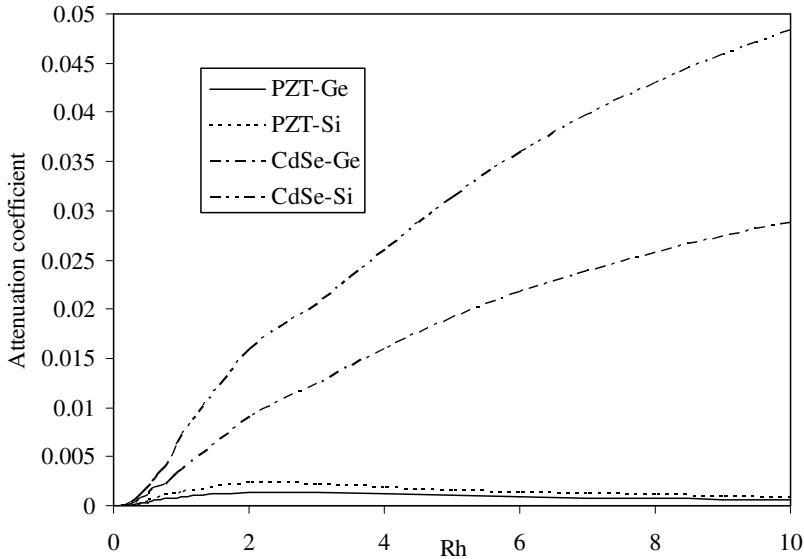
Figure 16. Attenuation coefficient versus *Rh* for PZT-Ge, PZT-Si, CdSe-Ge, and CdSe-Si composites.

magnitude in the composites with Ge cores as compared to those with Si. Moreover, the phase velocity attains a higher magnitude for the PZT patch than for the CdSe patch with the same choice of core material. The profiles of the attenuation coefficient follow similar trends in their variations for the same patch materials. In the case of the PZT patch, the attenuation initially increases to attain its maximum value and decreases afterwards with increasing wave number; it increases at all wave numbers for the CdSe patch. The attenuation coefficient possesses large values for the CdSe patch in comparison to that of the PZT patch for the same choice of core material. However, the attenuation is higher for the Si core than the Ge one. This shows that the PZT-Ge composite has low attenuation and high phase velocity, which indicates that the wave signal can travel longer distances in this structure. This is attributed to the fact that the characteristics of the composites consisting of thin-layered structures are dominated by the layer properties [Wang 2002; Trolier-Mckinstry and Muralt 2004]. Moreover, the generalised Rayleigh surface waves usually follow the interface surface as their guiding surface by causing less disturbance to the core material than in the patch. Thus the physical properties of the patch material play a more vital role in their propagation than those of the core. Hence, it is worth mentioning that the piezoelectric patch improves the functioning of surface wave devices (SAW) made up of semiconductor materials.

Conclusions

A functional iteration numerical technique along with Cardano's method has been successfully used to solve the complex secular equation in order to compute the phase velocities, attenuation coefficients, and specific loss factors of energy dissipation in CdSe-Si, CdSe-Ge, PZT-Si, and PZT-Ge composite structures. The phase velocity profiles show dispersive character in all the considered composites. Its magnitude decreases sharply at long wavelengths and becomes steady and uniform at short wavelengths. Higher-order modes of wave propagation have larger phase velocity compared to lower-order modes. In

CdSe-Si and CdSe-Ge composites, the attenuation as well as the specific loss factor of energy dissipation increase with increasing wave number, whereas both these quantities first increase and then decrease with increasing wave number in PZT-Si and PZT-Ge composites. Higher-order modes possess less attenuation and specific loss than lower-order ones. Phase velocity remains almost uniform in all the composites with the lifetime of the charge carriers. The attenuation in CdSe-Si and CdSe-Ge composites remains almost constant at short lifetimes and decreases with increasing lifetime. However, attenuation is noticed to be nearly constant in PZT-Si and PZT-Ge structures. In the n-type silicon halfspace, the phase velocity is noticed to be dispersive in nature. The attenuation profiles show oscillatory behaviour initially, then decrease after attaining maximum value, and finally become steady at large wave numbers for both types of considered boundary conditions. The specific loss factor also shows oscillatory behaviour at long wavelengths but becomes uniform at short wavelengths. Phase velocity remains constant at short lifetimes and increases at large values of the lifetime of the charge carrier field in the case where considered conditions prevail at the surface of semiconductor halfspace. The attenuation decreases with decreasing lifetime of the charge carriers for both types of boundary conditions. This study may be applicable to the design of piezoelectric thin-film devices.

Appendix

The coefficients a_{ij} used in (38) are given by

$$a_{13} = -P_3 \beta S_2 n_2 n^R - P_3(\beta p + ikq)p^S,$$

$$a_{1i} = (b_j - b_3)n^R + (y_j - y_3)p^S, \qquad\qquad i = 4, 5, \; j = i - 3,$$

$$a_{16} = \beta b_3 n^R + (q + \beta y_3)p^S,$$

$$a_{2i} = M_i P_3 - P_i M_3, \qquad\qquad i = 1, 2,$$

$$a_{23} = \{M_3 \beta S_2 - P_3(k^2 - \beta n_2)\}n^R - P_3(\beta p + ikq)p^N,$$

$$a_{2i} = (y_j - y_3)p^N, \qquad\qquad i = 4, 5, \; j = i - 3,$$

$$a_{26} = -ikn^R + (q + \beta y_3)p^N,$$

$$a_{3i} = d_i P_3 - P_i d_3, \qquad\qquad i = 1, 2,$$

$$a_{33} = \{d_3 \beta S_2 - P_3(ikp - \beta f_2)\}n^R - P_3(\beta p + ikq)p^F,$$

$$a_{3i} = (y_j - y_3)p^F, \qquad\qquad i = 4, 5, \; j = i - 3,$$

$$a_{36} = pn^R + (q + \beta y_3)p^F,$$

$$a_{41} = P_3 y_1 - P_1 y_3 \frac{\sinh(m_3 h)}{\sinh(m_1 h)},$$

$$a_{42} = P_3 y_2 \sinh(m_2 h) - P_2 y_3 \sinh(m_3 h),$$

$$a_{43} = \beta S_2 y_3 \sinh(m_3 h)n^R,$$

$$a_{4i} = \{y_i \cosh(m_i h) - y_3 \cosh(m_3 h)\}n^R, \qquad\qquad i = 4, 5, \; j = i - 3,$$

$$a_{46} = \beta y_3 \cosh(m_3 h)n^R,$$

$$a_{5i} = P_3 d_i \cosh(m_i h) - P_i d_3 \cosh(m_3 h), \quad i = 1, 2,$$
$$a_{53} = \beta S_2 d_3 \cosh(m_3 h) n^R,$$
$$a_{5i} = \{d_i \sinh(m_i h) - d_3 \sinh(m_3 h)\} n^R, \quad i = 4, 5, \ j = i - 3,$$
$$a_{56} = \beta d_3 \sinh(m_3 h) n^R,$$
$$a_{6i} = P_3 b_i \sinh(m_i h) - P_i b_3 \sinh(m_3 h), \quad i = 1, 2,$$
$$a_{63} = \beta S_2 b_3 \sinh(m_3 h) n^R,$$
$$a_{6i} = \{b_i \cosh(m_i h) - b_3 \cosh(m_3 h)\} n^R, \quad i = 4, 5, \ j = i - 3,$$
$$a_{66} = \beta b_3 \cosh(m_3 h) n^R,$$

where

$$n^R = (n_1^2 - n_2^2)(\beta p + ikq),$$
$$p^S = \beta S_2(S_1 n_1 - S_2 n_2) - \beta S_2 n_2(n_1^2 - n_2^2),$$
$$p^N = \beta S_2(n_2 - n_1) - (n_1^2 - n_2^2)(k^2 - \beta n_2),$$
$$p^F = \beta S_2(f_2 - f_1) - (n_1^2 - n_2^2)(ikp - \beta f_2).$$

References

[Bleustein 1968] J. L. Bleustein, "A new surface wave in piezoelectric materials", *Appl. Phys. Lett.* **13**:12 (1968), 412–414.

[Du et al. 2007] J. Du, X. Jin, J. Wang, and K. Xian, "Love wave propagation in functionally graded piezoelectric material layer", *Ultrasonics* **46**:1 (2007), 13–22.

[Graff 1975] K. F. Graff, *Wave motion in elastic solids*, Clarendon Press, Oxford, 1975.

[Gulyaev 1969] Y. V. Gulyaev, "Electroacoustic surface waves in solids", *JETP Letters* **9**:1 (1969), 37–38.

[Jin et al. 2002] J. Jin, Q. Wang, and S. T. Quek, "Lamb wave propagation in a metallic semi-infinite medium covered with piezoelectric layer", *Int. J. Solids Struct.* **39**:9 (2002), 2547–2556.

[Kagan 1997] V. D. Kagan, "Propagation of a surface acoustic wave in a layered system containing a two-dimensional conducting layer", *Semiconductors* **31**:4 (1997), 407–410.

[Kolsky 1963] H. Kolsky, *Stress waves in solids*, Dover Press, New York, 1963.

[Liu et al. 2004] H. Liu, J. J. Lee, and Z. M. Cai, "Analysis of nonlinear acoustoelastic effect of surface acoustic waves in laminated structures by transfer matrix method", *Mech. Res. Commun.* **31**:6 (2004), 667–675.

[de Lorenzi and Tiersten 1975] H. G. de Lorenzi and H. F. Tiersten, "On the interaction of the electromagnetic field with heat conducting deformable semiconductors", *J. Math. Phys.* **16**:4 (1975), 938–957.

[Lowrie 2007] W. Lowrie, *Fundamental of geophysics*, Cambridge University Press, New York, 2007.

[Maruszewski 1989] B. Maruszewski, "Thermodiffusive surface waves in semiconductors", *J. Acoust. Soc. Am.* **85**:5 (1989), 1967–1977.

[Maugin and Daher 1986] G. A. Maugin and N. Daher, "Phenomenological theory of elastic semiconductors", *Int. J. Eng. Sci.* **24**:5 (1986), 703–731.

[Melkumyan and Mai 2009] A. Melkumyan and Y.-w. Mai, "Electroelastic gap waves between dissimilar piezoelectric materials in different classes of symmetry", *Int. J. Solids Struct.* **46**:21 (2009), 3760–3770.

[Muralt and Baborowski 2004] P. Muralt and J. Baborowski, "Micromachined ultrasonic transducers and acoustic sensors based on piezoelectric thin films", *J. Electroceramics* **12**:1-2 (2004), 101–108.

[Rayleigh 1885] L. Rayleigh, "On waves propagated along the plane surface of an elastic solid", *Proc. London Math. Soc.* **7**:1 (1885), 4–11.

[Sharma and Pal 2004] J. N. Sharma and M. Pal, "Propagation of Lamb waves in a transversely isotropic piezothermoelastic plate", *J. Sound Vib.* **270**:4-5 (2004), 587–610.

[Sharma and Pathania 2006] J. N. Sharma and V. Pathania, "Thermoelastic waves in coated homogeneous anisotropic materials", *Int. J. Mech. Sci.* **48**:5 (2006), 526–535.

[Sharma and Thakur 2006] J. N. Sharma and N. Thakur, "Plane harmonic elasto-thermodiffusive waves in semiconductor materials", *J. Mech. Mater. Struct.* **1**:5 (2006), 813–835.

[Sharma et al. 2007] J. N. Sharma, N. Thakur, and S. Singh, "Propagation characteristics of elasto-thermodiffusive surface waves in semiconductor material half-space", *J. Therm. Stresses* **30**:4 (2007), 357–380.

[Sharma et al. 2009] J. N. Sharma, N. Thakur, and S. Singh, "Elasto-thermodiffusive (ETNP) surface waves in semiconductor materials", *Int. J. Solids Struct.* **46**:11-12 (2009), 2309–2319.

[Sharma et al. 2010] J. N. Sharma, K. K. Sharma, and A. Kumar, "Surface waves in a piezoelectric-semiconductor composite structure", *Int. J. Solids Struct.* **47**:6 (2010), 816–826.

[Trolier-Mckinstry and Muralt 2004] S. Trolier-Mckinstry and P. Muralt, "Thin film piezoelectrics for MEMS", *J. Electroceramics* **12**:1-2 (2004), 7–17.

[Wang 2002] Q. Wang, "Wave propagation in a piezoelectric coupled solid medium", *J. Appl. Mech.* (*ASME*) **69**:6 (2002), 819–824.

[Wang and Varadan 2002] Q. Wang and V. K. Varadan, "Wave propagation in piezoelectric coupled plates by use of interdigital transducer, I: dispersion characteristics", *Int. J. Solids Struct.* **39**:5 (2002), 1119–1130.

[White 1967] R. M. White, "Surface elastic-wave propagation and amplification", *IEEE Trans. Electron Devices* **14**:4 (1967), 181–189.

J. N. SHARMA: jns@nitham.ac.in
Department of Mathematics, National Institute of Technology, Hamirpur 177005, India

K. K. SHARMA: kks@nitham.ac.in
Department of Physics, National Institute of Technology, Hamirpur 177005, India

ASHWANI KUMAR: puri_nit@yahoo.com
Department of Physics, National Institute of Technology, Hamirpur 177005, India

JOURNAL OF MECHANICS OF MATERIALS AND STRUCTURES

jomms.org

Founded by Charles R. Steele and Marie-Louise Steele